Міністерство освіти і науки України
Чернівецький національний університет
імені Юрія Федьковича

Інститут фізико-технічних та комп'ютерних наук
Кафедра електроніки і енергетики

Розробка сонячних елементів на основі структур TiN/InP/графіт

Кваліфікаційна робота
ОКР «Бакалавр»

Виконав: студент 4 курсу, групи 433і
спеціальності 141 Електроенергетика,
електротехніка та електромеханіка
Мохамед Абдельвадуд
Керівник Солован М.М._____
Рецензент _____

До захисту допущено:
Протокол засідання кафедри № __
від „___" _____ 2021 р.
зав. кафедри_____доц. Майструк Е. В.

Чернівці–2021

Ministry of Education and Science of Ukraine

Yuri Fedkovych Chernivtsi National University

Institute of Physical, Technical and Computer Sciences

Department of Electronics and Energy

Development of solar cells based on structures

TiN / InP / Graphite "

Graduate work

"Bachelor"

Completed: 4th year student, group 433i specialties 141 Electric power, electrical engineering and electromechanics (code and name of the specialty)

Mohamed Abdelwadood

Supervisor Solovan M.M.

Chernivtsi

2021

Анотація

В даній роботі представлені результати досліджень можливості розробки сонячних елементів на основі структури TiN / InP / Graphite .

На даний час є актуальним завданням перед експериментальними роботами виконувати комп’ютерне моделювання запланованих сонячних елементів для всебічного розуміння фотоелектричних процесів у досліджуваних нових сонячних елементах. Зокрема, ми використовували сучасні методи оптичного та електричного моделювання. Ці методи чисельного моделювання наддадуть детальну інформацію про швидкість фотогенерації вільних носіїв заряду в залежності від товщини поглинача та довжини хвилі. В роботі запропоновано сонячні елементи на основі структур TiN/InP/графіт. Визначено швидкість фотогенерації вільних носіїв заряду в залежності від товщини поглинача та довжини хвилі в сонячних елементах TiN/InP/графіт. Встановлено, що в сонячних елементах на основі TiN/InP/графіт оптимальною товщиною поглинача (InP) становить 300 нм. Показано, що сонячні елементи TiN/InP/графіт будуть володіти широкою областю спектральної чутливості (від 300 до 850 нм).

Робота написана на англійській мові і містить 51 сторінку, 22 рисунки, 1 таблицю і 9 літературних джерел.

Content

Introduction

A solar cell, or photovoltaic cell, is an electrical device that converts the energy of light directly into electricity by the photovoltaic effect, which is a physical and chemical phenomenon. It is a form of photoelectric cell, defined as a device whose electrical characteristics, such as current, voltage, or resistance, vary when exposed to light. Individual solar cell devices are often the electrical building blocks of photovoltaic modules, known colloquially as solar panels. The common single junction silicon solar cell can produce a maximum open-circuit voltage of approximately 0.5 to 0.6 volts.

Solar cells are described as being photovoltaic, irrespective of whether the source is sunlight or an artificial light. In addition to producing energy, they can be used as a photodetector (for example infrared detectors), detecting light or other electromagnetic radiation near the visible range, or measuring light intensity.

The operation of a photovoltaic (PV) cell requires three basic attributes:

- The absorption of light, generating either electron-hole pairs or excitons.
- The separation of charge carriers of opposite types.
- The separate extraction of those carriers to an external circuit.

In contrast, a solar thermal collector supplies heat by absorbing sunlight, for the purpose of either direct heating or indirect electrical power generation from heat. A "photoelectrolytic cell" (photoelectrochemical cell), on the other hand,

refers either to a type of photovoltaic cell (like that developed by Edmond Becquerel and modern dye-sensitized solar cells), or to a device that splits water directly into hydrogen and oxygen using only solar illumination.

Indium phosphide can be prepared from the reaction of white phosphorus and indium iodide at 400 °C. also by direct combination of the purified elements at high temperature and pressure, or by thermal decomposition of a mixture of a trialkyl indium compound and phosphine.

InP is used in high-power and high-frequency electronics because of its superior electron velocity with respect to the more common semiconductors silicon and gallium arsenide.

It was used with indium gallium arsenide to make a record breaking pseudomorphic heterojunction bipolar transistor that could operate at 604 GHz.

It also has a direct bandgap, making it useful for optoelectronics devices like laser diodes. The company Infinera uses indium phosphide as its major technological material for manufacturing photonic integrated circuits for the optical telecommunications industry, to enable wavelength-division multiplexing applications.

InP is also used as a substrate for epitaxial indium gallium arsenide based opto-electronic devices.

At present, it is an urgent task to perform computer simulations of planned solar cells before experimental work for a comprehensive understanding of photoelectric processes in the studied new solar cells. In particular, we used modern methods of optical and electrical modeling. These numerical simulation methods will provide detailed information on the rate of photogeneration of free charge carriers depending on the absorber thickness and wavelength.

SECTION 1. Theoretical part

1.1 Physical properties of graphite thin films and indium phosphide (InP) and their application in solar energy

1.1.1 Methods of deposition of graphite thin films

The graphite films were grown by chemical vapor deposition technique from a hydrogen–methane gas mixture activated by DC discharge. A detailed description of the deposition facility and the growth method has been done elsewhere . Our CVD system allows production of different types of carbon films ranging from polycrystalline diamond to carbon nanotubes. A type of the material deposited depends essentially on the methane concentration and on the substrate temperature. In this work, the process parameters corresponding to graphite phase deposition have been chosen : the gas mixture composition H_2:CH_4 = 92:8; the total gas pressure P = 80 Torr; the substrate temperature of 950 C. In these conditions the nano-graphite meso-porous layers were deposited after 1–1.5 h . The deposition procedure includes pumping out the reactor chamber by a rotary pump to the base pressure value of 103 Torr followed by introduction of a pure hydrogen and ignition of DC discharge at pressure of about 40 Torr. Then the hydrogen pressure was increased up to 80 Torr simultaneously with increasing the discharge current. This procedure took about 10 min. It was followed by an introduction of the methane gas into the reactor and an increase of its content up to 8 vol%. The

discharge current was fixed at value about 0.5 A/cm^2 being typical for the graphite phase formation . Optical emission spectra (OES) measured in DC discharge plasma have revealed an important role of carbon dimers C2 generated in the plasma near the substrate surface. The dimers may be considered as building blocks for the graphite deposit [1]. In present study the deposition time has been reduced to 5–10 min to obtain the thinner films. In our CVD system the main parameters are stabilized usually not earlier than 15 min after the process starts. Thus, the process is not completely under control during first minutes of deposition. For instance, the intensities of OES peaks (including those corresponding to C_2 dimers) are varied with time in contrast to the fixed values observed in case of the standard deposition conditions. However, the deposition procedure has shown surprisingly good repeatability of the results despite of the incontrollable character of its initial stage. In this work, the silicon and nickel square plates with thickness of about 0.5 mm and lateral dimensions of 10·10 mm or 25·25 mm were used as substrates. The single crystalline silicon substrates have been prepared by cutting the standard polished Si wafers. The nickel substrates were made by cutting of the polycrystalline Ni sheets with thickness of 0.5 mm produced by rolling. The substrates were treated in pure hydrogen DC plasma to remove the surface oxide layer before the interaction with methane started. The CVD-deposited graphite films were studied by Raman spectroscopy using a Fourier-transform Raman apparatus Bruker FR 1·10^6 with excitation by a YAG:Nd laser operating at wavelength 1064 nm. A special care has been taken to avoid the material heating by laser radiation in course of measurements. For this purpose the Raman spectra were first measured with different laser power densities. The final level of the laser power density was chosen in the middle of the range where no temporal changes in the line positions and shapes were observed. Raman spectra of HOPG sample (HOPG SPI-3 GRADE supplied by SPI, West Chestr, PA 19381,

USA) were recorded at the same conditions to obtain the reference data. The surface morphology was studied with a scanning electron microscopy (SEM) using LEO Supra 50 PV instrument and a scanning tunneling microscopy (STM). An Auger electron spectroscopy (AES) was used for elemental analysis of the surface. The AES and STM measurements were carried out at room temperature under ultra-high vacuum (UHV) conditions in a multi-chamber setup equipped with a cylindrical mirror analyzer Riber OPS-200 (for AES), Sigma Scan GPI-300 (for STM) and other instruments for the surface analysis and treatments. A basic pressure in the setup did not exceed $2 \cdot 10^{10}$ Torr. A preparation of W-tips for STM measurements was made by an electrochemical etching outside and a subsequent sharpening inside the vacuum chamber with Ar^{+}-bombardment . The samples were investigated by AES and STM in ‘‘as grown’’ form (without any UHV treatments)

Raman spectroscopyis a spectroscopic technique typically used to determine vibrational modes of molecules, although rotational and other low-frequency modes of systems may also be observed. Raman spectroscopy is commonly used in chemistry to provide a structural fingerprint by which molecules can be identified. Raman spectroscopy relies upon inelastic scattering of photons, known as Raman scattering. A source of monochromatic light, usually from a laser in the visible, near infrared, or near ultraviolet range is used, although X-rays can also be used. The laser light interacts with molecular vibrations, phonons or other excitations in the system, resulting in the energy of the laser photons being shifted up or down. The shift in energy gives information about the vibrational modes in the system. Infrared spectroscopy typically yields similar yet complementary information.

Typically, a sample is illuminated with a laser beam. Electromagnetic radiation from the illuminated spot is collected with a lens and sent through

a monochromator. Elastic scattered radiation at the wavelength corresponding to the laser line (Rayleigh scattering) is filtered out by either a notch filter, edge pass filter, or a band pass filter, while the rest of the collected light is dispersed onto a detector. Spontaneous Raman scattering is typically very weak; as a result, for many years the main difficulty in collecting Raman spectra was separating the weak inelastically scattered light from the intense Rayleigh scattered laser light (referred to as "laser rejection"). Historically, Raman spectrometers used holographic gratings and multiple dispersion stages to achieve a high degree of laser rejection. In the past, photomultipliers were the detectors of choice for dispersive Raman setups, which resulted in long acquisition times. However, modern instrumentation almost universally employs notch or edge filters for laser rejection. Dispersive single-stage spectrographs (axial transmissive (AT) or Czerny–Turner (CT) monochromators) paired with CCD detectors are most common although Fourier transform (FT) spectrometers are also common for use with NIR lasers.

The name "Raman spectroscopy" typically refers to vibrational Raman using laser wavelengths which are not absorbed by the sample. There are many other variations of Raman spectroscopy including surface-enhanced Raman, resonance Raman, tip-enhanced Raman, polarized Raman, stimulated Raman, transmission Raman, spatially-offset Raman, and hyper Raman.

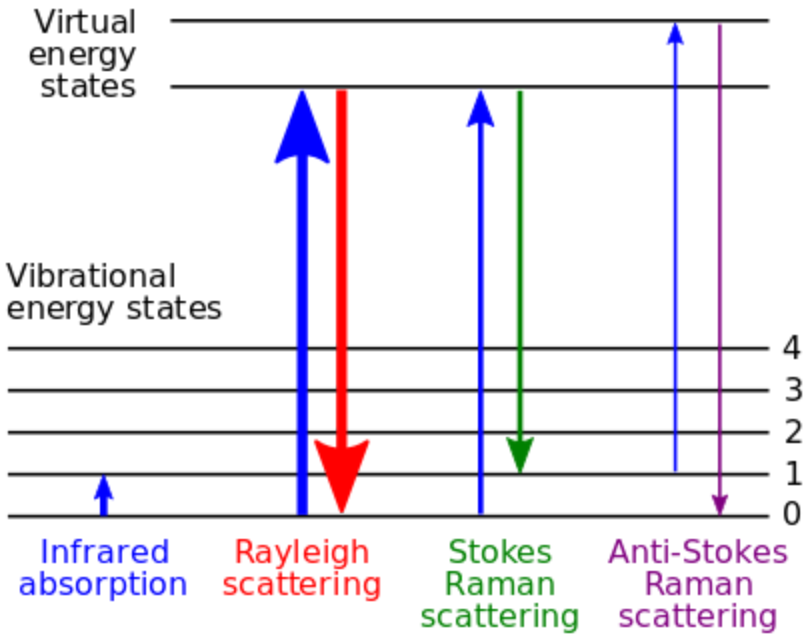

Fig.1.1. Energy-level diagram showing the states involved in Raman spectra

Auger electron spectroscopy is a common analytical technique used specifically in the study of surfaces and, more generally, in the area of materials science. Underlying the spectroscopic technique is the Auger effect, as it has come to be called, which is based on the analysis of energetic electrons emitted from an excited atom after a series of internal relaxation events. The Auger effect was discovered independently by both Lise Meitner and Pierre Auger in the 1920s. Though the discovery was made by Meitner and initially reported in the journal Zeitschrift für Physik in 1922, Auger is credited with the discovery in most of the scientific community[2]. Until the early 1950s Auger transitions were considered nuisance effects by spectroscopists, not containing much relevant material information, but studied so as to explain anomalies in X-ray spectroscopy data. Since 1953 however, AES has become a practical and straightforward characterization technique for probing chemical and compositional

surface environments and has found applications in metallurgy, gas-phase chemistry, and throughout the microelectronics industry.

The UV Excimer laser of wavelength 248 nm, pulse width of 20 ns and Pulse energy 13-50 mJ focused tightly with the help of UV lens of focal length ~ 40cm. The laser pulse has been focused at an angle 45° to irradiate 4N pure graphite solid target. To avoid crater step motor has been used to rotate graphite target continuously during laser ablation. The silicon substrate (of dimension 2x2 cm^2) has placed at distance of 15 mm normal to the target surface. The in 8-port stainless steel chamber with vacuum system has been used to deposit thin film and the films were deposited under pressure of ~ 10^{-4} Torr, maintained by rotary and turbo molecular pump. Graphite thin films have been frown at two different substrate temperature 25°C (room temperature) and 300°C which has been achieved by hydrogen lamp. Each film has been grown on the substrate for 10,000 laser shorts. The structural and surface analysis of deposited thin films has done by XRD and SEM respectively. The schematic diagram for experimental setup has shown in Figure 1.2.

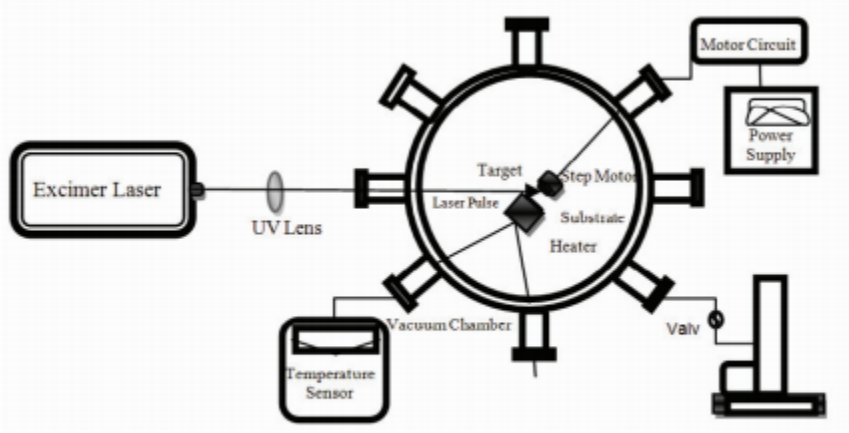

Figure 1.2 : schematic of the experimental setup

The Figures 1.3 (a & b) illustrate the XRD pattern of Carbon thin films deposited by pulse laser deposition (PLD) on Si substrates at temperatures 25°C and 300°C respectively. The XRD graphs show that the two thin films deposited at substrate temperature 25°C and 300°C have amorphous structure however the film deposited at high substrate temperature shows some crystallinity. The higher substrate temperature of substrate is in favor to the diffusion of atoms absorbed on the substrate surface and accelerates. The high substrate temperature favor the migration of incident atoms or molecules to the energy favorable positions, resulting in the enhancement of the smoothness of film, which results the increase of peak strength and decrease of full-width and the half-maximum (FWHM) value. Table 1 shows the structural parameters as particle size, d-spacing and the value of FWHM corresponding to angle 2θ. It is found that the strength of peak increases and FWHM value decreases with increase in substrate temperature as the intensity of peak corresponding to angle 2θ = 6.2° increases while the value of FWHM decreases form 0.72 to 0.59. The structural parameters are calculated using the standard Debye-Scherrer formula . (0.94) cos D λ β θ × = (1) where λ is the wavelength of X-ray, D is the particle size and 2θ is the angle between the incident and the scattered X-rays.

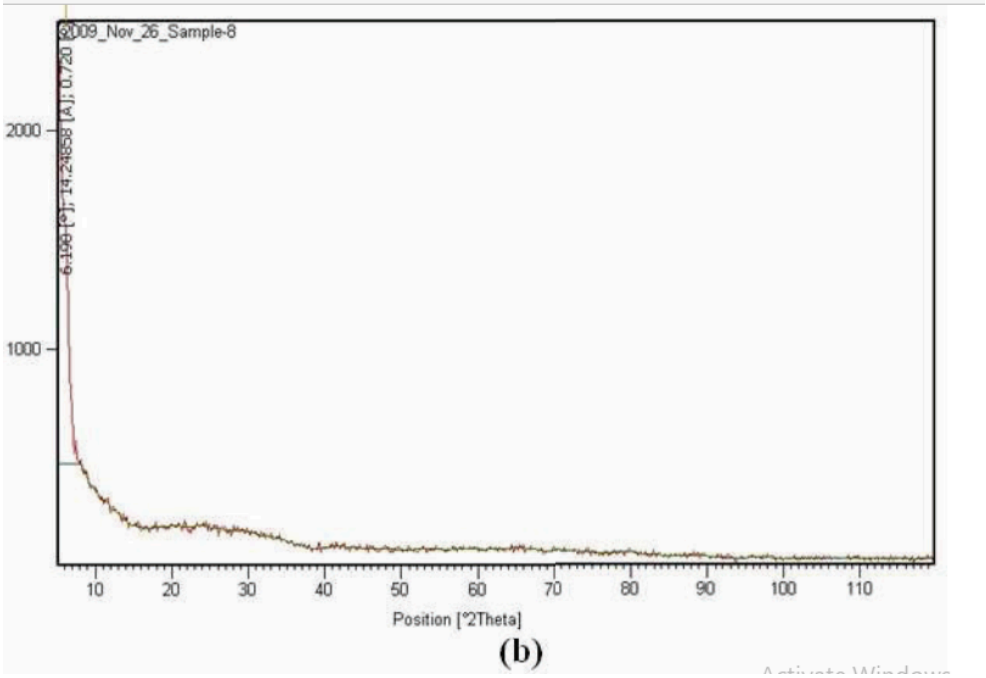

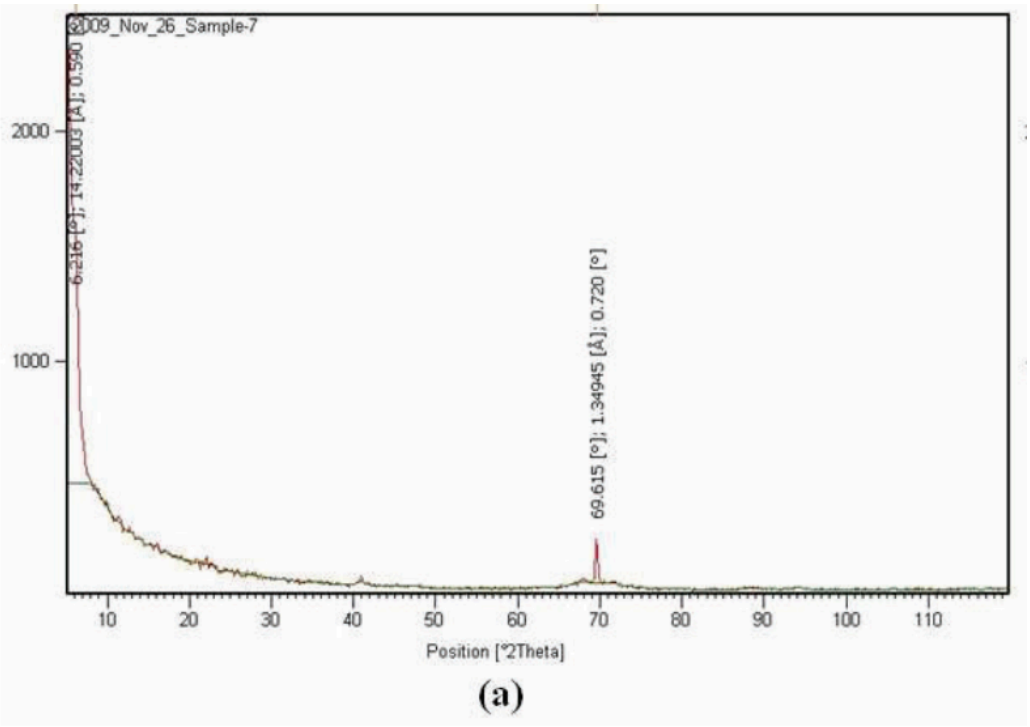

Figure 1.3:XRD image of a C thin film Si substrate 25^{o}C and $300^{o}C$

Table 1: XRD data for C thin film at room

Temperature(25^0C)						
NO	Position $[20^0]$	I_P(counts)	I_r=(I/MAX) 100	d-spacing $[A^0]$	FWHM $[20^0]$	Particle Size(mn)
1	6.2	468	100	14.2	0.59	12.3
2	69.6	36	18.63	1.3	0.72	10.88
Temperature(300^0C)						
3	6.1	458	100	14.2	0.72	10.88

FWHM value of XRD patterns shows with the increase in substrate temperature the dislocation density decreases and many dislocations are annihilated or moved into lower energy configuration. The above results show that the uniformity of the deposited films increases with higher substrate temperature.

1.1.2 Structural and electrical properties of graphite thin films

Materials and Methods Large-area coatings of graphite-based materials were deposited on LDPE substrates (20 × 30 cm^2) by spray coating technology, using a commercial lacquer, Graphit 33 (from Kontakt Chemie, Zele, Belgium), which is commonly used for optical and electrical applications. During spraying, the full cone jet spot was horizontally directed on the film taking a distance of 20 cm. After spraying, the coated substrates were dried in air at room temperature, for 4 h. In order to investigate the morphological and structural properties of the samples, scanning electron microscopy (SEM) was performed using a FEI Quanta 200 FEG

microscope and X-ray diffraction (XRD) measurements were carried out by a Panalytical, X'PERT PRO diffractometer with a Cu-Kα radiation source (λ = 1.5406 Å). Electrical properties were studied by means of measurements under vacuum in a coplanar configuration by silver paint contacts (1 cm long and 1 mm spaced) spread on the top sample surfaces. Vacuum was applied to prevent possible effects of moisture or other adsorbates. Currentvoltage (I-V) characteristics were taken in a Janis Research ST-500 probe station, equipped with 4 micromanipulators connected to a Source-Measurement Unit (SMU) Keithley 4200-SCS (Tektronix, Inc., Beaverton, OR, USA). The electrical resistance, R, of the samples at different temperatures, T, was measured during heating runs from 20 °C to 120 °C at a rate of about 5 °C/min. The mean values of resistance were estimated by monitoring R on a period of 60 s.

X-ray diffraction, a phenomenon in which the atoms of a crystal, by virtue of their uniform spacing, cause an interference pattern of the waves present in an incident beam of X rays. The atomic planes of the crystal act on the X rays in exactly the same manner as does a uniformly ruled grating on a beam of light.

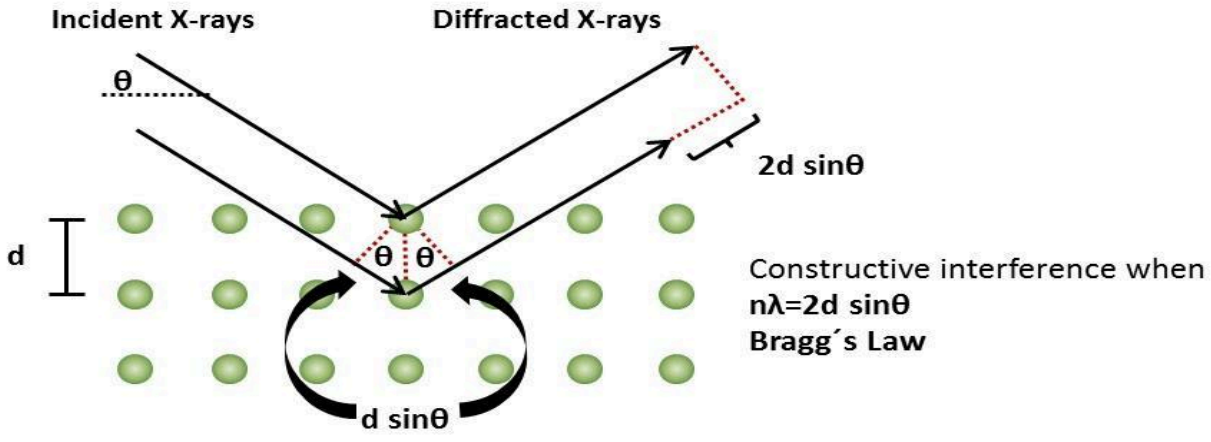

Figure 1.4: Schematic representation of the bragg equation

SEM-micrographs in Figure 1.5 show that the coating obtained by spraying Graphit 33 lacquer on LDPE substrate is quite rough, porous, and made of small platelets well connected together.

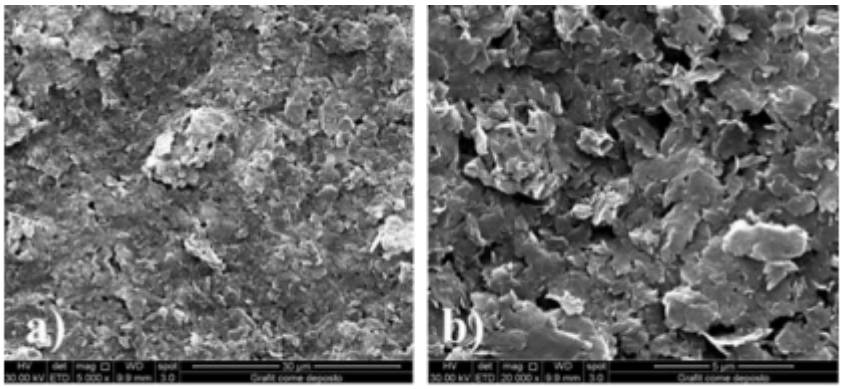

Fig. 1.5 SEM-micrograps of the`as deposited coating spraying Graphite

X-ray diffraction is a powerful nondestructive technique for characterizing crystalline materials. It provides information on structures, phases, preferred crystal orientations (texture), and other structural parameters, such as average grain size, crystallinity, strain, and crystal defects. XRD peaks are produced by constructive interference of a monochromatic beam of X-rays scattered at specific angles from each set of lattice planes in a sample. The peak intensities are determined by the atomic positions within the lattice planes. Consequently, the XRD pattern is the fingerprint of periodic atomic arrangements in a given material. An online search of a standard database for X-ray powder diffraction patterns enables quick phase identification for a large variety of crystalline samples.

XRD technique utilizes the X-ray scattering phenomenon to elucidate the crystal structure of crystalline/semicrystalline materials, with scattering of X-rays by periodic array of atoms giving rise to definite diffraction patterns that bestows a qualitative image of atomic arrangements within the crystal lattice. Powder X-Ray

Diffraction (P-XRD) is one such characterization tool that offers the advantage of simultaneous characterizing of both the precursor and end products with a detailed qualitative presentation of their micro-structural behaviours. It is the most sought after and convenient technique towards the characterization of polymer based nanocomposite in contrast to single crystal technique, which demands the sample in the form of individual/single/independent crystals. Furthermore, XRD is a versatile, non-destructive characterization technique that offers a thorough output of chemical composition and hence the crystallographic structure of materials .

XRD is the most commonly used method to investigate the structural features of nanocomposites due to its ease and availability. XRD is used to evaluate the crystalline structure, the ratio of crystalline to non-crystalline (amorphous) regions, crystal size, the arrangement pattern of crystals and the distance between the planes of the crystal . This means that structural changes induced in a crystalline material by blending with other materials can be monitored using the XRD technique. Mazhar Ul-Islama et al. have investigated the micro-structural changes using XRD in the BC sheets caused by the adsorption and penetration of MMT particles. The XRD patterns of BC (bacterial cellulose), MMT (montmorillolite), BC–MMT1, BC–MMT2 and BC–MMT3 are shown in Fig. 1.6. The BC–MMT composites (BC–MMT1, BC–MMT2 and BC–MMT3) were prepared by impregnation of BC sheets in respective concentrations (1, 2 and 4%) of MMT suspensions at 150 rpm for 24 h. The smaller angle (7–10 degrees) XRD patterns for all these samples have been shown in the upper left corner.

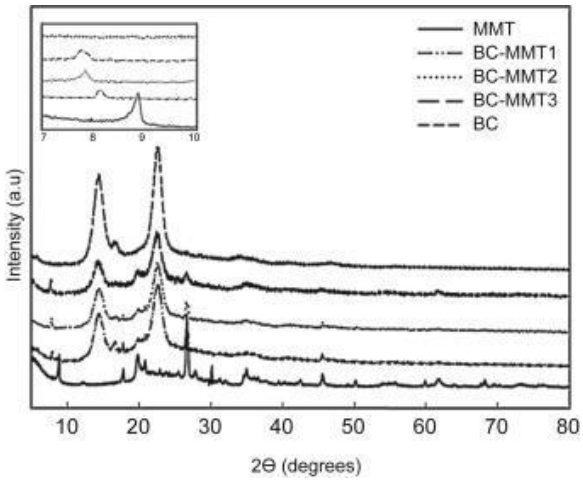

Fig. 1.6 XRD patterns of pure BC, pure MMT, BC–MMT1, BC–MMT2 and BC–MMT3.

In general, the rate of crystallization and the degree of crystallinity are affected by the addition of fillers. *M.A. Lopez Manchado et al.* have used single-walled nanotubes (SWNTs) as filler. However, no significant change in the polypropylene (PP) crystalline structure was observed in the presence of SWNTs, as shown in Fig. 1.7.

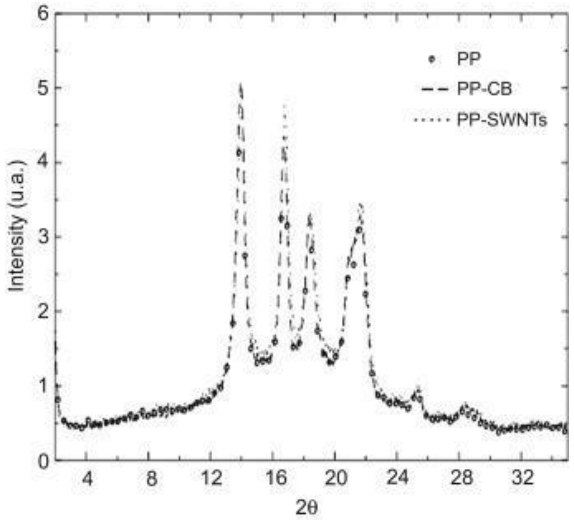

Fig. 1.7. X-ray diffractograms of pure PP and its composites filled with 0.5 wt%.

The set of reflections proves unambiguously that isotactic polypropylene (iPP) remains primarily in monoclinic form . These changes in PP crystallization from the addition of carbon nanotubes are of crucial importance for interpreting the mechanical behaviour of the composites.

Large area GP films were deposited on LDPE substrates by a spray coating technology, using a graphite lacquer. SEM images and XRD analysis show that the films consist of overlapped graphite platelets composed of crystallites with an average size of 13.6 nm in the (002) direction. The electrical characterization of the samples, as a function of temperature suggests that the thermal properties of the LDPE substrate (thermal expansion and phase transition), strongly affect the thermoresistive properties of GP films. The resistance of the GP film on LDPE considerably increases in the 20–100 °C range, but sharply decreases above the temperature of 100 °C. The investigated material could be used as temperature sensor in the thermal ranges where the polymeric substrate remains still solid.

1.1.3 Physical properties of InP single-crystal

A new route to grow an ensemble of indium phosphide single-crystal semiconductor nanowires is described. Unlike conventional epitaxial growth of single-crystal semiconductor films, the proposed route for growing semiconductor nanowires does not require a single-crystal semiconductor substrate. In the proposed route, instead of using single-crystal semiconductor substrates that are characterized by their long-range atomic ordering, a template layer that possesses short-range atomic ordering prepared on a non-single-crystal substrate is employed. On the template layer, epitaxial information associated with its short-range atomic ordering is available within an area that is comparable to that of

a nanowire root. Thus the template layer locally provides epitaxial information required for the growth of semiconductor nanowires. In the particular demonstration described in this paper, hydrogenated silicon was used as a template layer for epitaxial growth of indium phosphide nanowires. The indium phosphide nanowires grown on the hydrogenerated silicon template layer were found to be single crystal and optically active. Simple photoconductors and pin-diodes were fabricated and tested with the view towards various optoelectronic device applications where group III–V compound semiconductors are functionally integrated onto non-single-crystal platforms.

High-quality single-crystal substrates have been used for epitaxial growth of high-quality semiconductor films when large area is required for device fabrication. As a result, significant efforts have been dedicated to developing epitaxial growth processes that produce semiconductor films that are homogeneous in composition and uniform in thicknesses over required area. Even in the synthesis of nanometerscale semiconductor structures such as quantum dots and nanowires, the use of single-crystal substrates is very common. For example, self-organized InAs quantum dots have been extensively studied on single-crystal GaAs (100) . Epitaxial growth of semiconductor nanowires generally makes use of single-crystal substrates. The growth of group III–V compound semiconductor nanowires has been demonstrated almost exclusively on single-crystal substrates. In Particular, GaAs or InP nanowires were grown on singlecrystal group III–V compound semiconductor substrates or on single-crystal Si substrates . In the growth of semiconductor nanowires on single-crystal substrates, the surface of a single-crystal substrate provides epitaxial information (e.g., crystallographic symmetries and lattice constants,

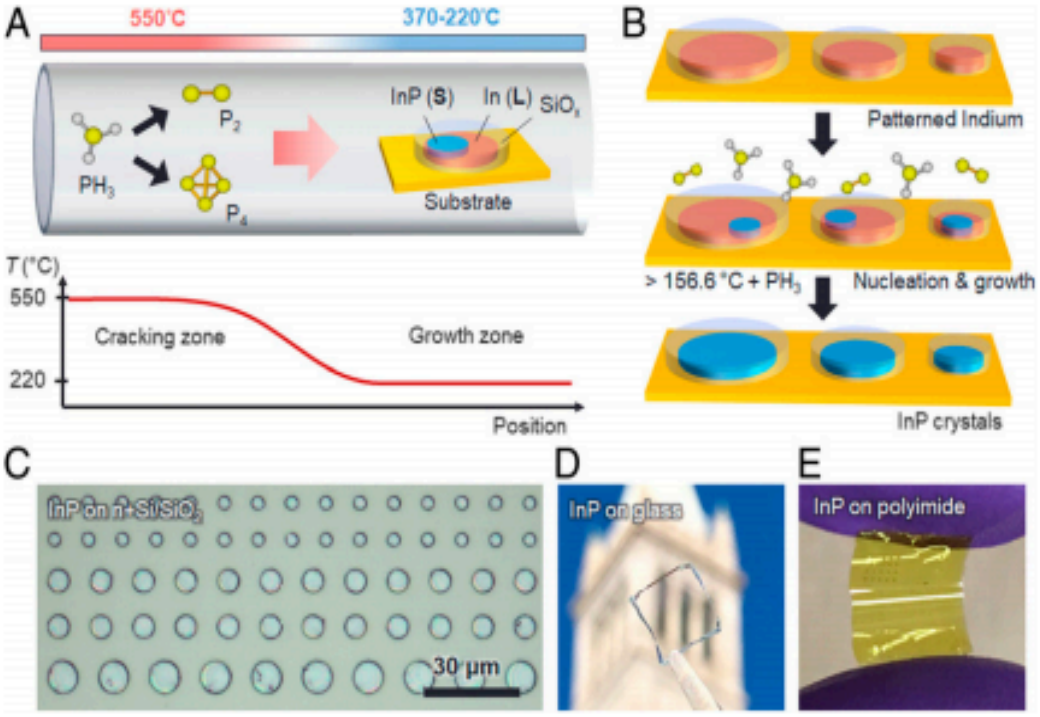

Fig.1.8. LT-TLP growth of InP (A) Schematic of the LT-TLP process where the sample is placed at low temperatures while the gas is cracked at high temperature. S indicates the solid phase L liquid (B) Schematic of the InP nuclertion and growth processes (C-E) images of as-grown of as-grown InP patterms on n+SuSiO2 ITO coated glass and peeled polyimide.

Single-crystal patterned growth is enabled with the probability dependent on the ratio of the depletion length to feature size. Optical images of patterned InP circles (thickness, ~300 nm; diameter, 3 to 7 µm) grown on Si/SiO^2 at 270 °C are shown in Fig. 1C. The low growth temperature characteristic of the LTTLP method allows for direct growth of InP on an unprecedented range of substrates. As a proof of concept, InP patterns were directly grown on indium-tin-oxide (ITO)-coated soda-lime glass (Fig. 1D) and polyimide substrates (Fig. 1.8E), both of which are thermally incompatible with traditional III–V deposition techniques such as MBE and MOCVD. While 220 °C is the lowest growth temperature used in this work to

assess material quality, we note that nucleation and growth occur at temperatures as low as 180 °C (SI Appendix,), demonstrating the flexibility of this method for a wide range of applications in flexible and transparent electronics.

A new route to grow an ensemble of indium phosphide single-crystal semiconductor nanowires is described. Unlike conventional epitaxial growth of single-crystal semiconductor films, the proposed route for growing semiconductor nanowires does not require a single-crystal semiconductor substrate. In the proposed route, instead of using single-crystal semiconductor substrates that are characterized by their long-range atomic ordering, a template layer that possesses short-range atomic ordering prepared on a non-single-crystal substrate is employed. On the template layer, epitaxial information associated with its short-range atomic ordering is available within an area that is comparable to that of a nanowire root. Thus the template layer locally provides epitaxial information required for the growth of semiconductor nanowires. In the particular demonstration described in this paper, hydrogenated silicon was used as a template layer for epitaxial growth of indium phosphide nanowires. The indium phosphide nanowires grown on the hydrogenerated silicon template layer were found to be single crystal and optically active. Simple photoconductors and pin-diodes were fabricated and tested with the view towards various optoelectronic device applications where group III–V compound semiconductors are functionally integrated onto non-single-crystal platforms.

Crystal growth

A crystal is a solid material whose constituent atoms, molecules, or ions are arranged in an orderly repeating pattern extending in all three spatial dimensions. Crystal growth is a major stage of a crystallization process, and

consists in the addition of new atoms, ions, or polymer strings into the characteristic arrangement of the crystalline lattice. The growth typically follows an initial stage of either homogeneous or heterogeneous (surface catalyzed) nucleation, unless a "seed" crystal, purposely added to start the growth, was already present.

The action of crystal growth yields a crystalline solid whose atoms or molecules are close packed, with fixed positions in space relative to each other. The crystalline state of matter is characterized by a distinct structural rigidity and very high resistance to deformation (i.e. changes of shape and/or volume). Most crystalline solids have high values both of Young's modulus and of the shear modulus of elasticity. This contrasts with most liquids or fluids, which have a low shear modulus, and typically exhibit the capacity for macroscopic viscous flow.

1.1.4 Physical properties of TiN thin films

In paper [] reports on the characterization of films of titanium nitride (TiN) obtained by reactive sputtering of titanium in a nitrogen-rich ambient (r.f. sputtering) and by nitrogen implantation during vapour deposition of titanium thin films.

In order to get a complete picture of the properties of the atoms in these systems the thin films were characterized with Auger electron spectroscopy and with a Seeman-Bohlin X-ray diffractometer. The overlayers were analysed by four-point probe to evaluate the resistivity.

The observed chemical and physical properties of the films strongly depend on both the growth technique and the particular parameters employed.

Recent years have seen an intensive search for and investigation of various materials potentially attractive for application in highefficiency photoelectric devices. Titanium nitride (TiN) is a promising wideband gap material. It possesses

an advantageous combina tion of physicochemical parameters: low resistivity, rather high transmission in the visible range, high reflectance in the infrared spectral region, high hard ness, high wear resistance, good chemical inertness, and good corrosion resistance .Titanium nitride is used in optical filters, thinfilm resistors, and protective and decorative coatings . Owing to its physical properties, TiN is an attrac tive material for application in various photoelectric devices , so the study of the optical and electrical properties of thin titanium nitride films is of consider able interest. Results of studies of some properties of thin TiN films were presented in many reports , but, to the best of our knowledge, no detailed studies of elec trical contacts to TiN thin semiconductor films or optical or electrical properties of transparent or con ductive TiN thin films have been reported in the liter ature. Such studies would be very helpful for further optimization of heterojunctionbased devices for elec tronics and solar power conversion because the effi ciency of such devices is significantly influenced by the optical and electrical characteristics of heterojunc tion components . In this paper, we report the optical and electrical properties of TiN thin films produced by reactive mag netron sputtering. EXPERIMENTAL TiN thin films were grown on precleaned glass and glassceramic substrates in a LeyboldHeraeus L560 multipurpose vacuum system by dc reactive magne tron sputtering of a pure (99.99%) titanium target in an argon + nitrogen atmosphere. The titanium target, in the form of a disk 100 mm in diameter and 5 mm in thickness, was placed on the stage of a watercooled magnetron 7 cm below sub strates. The glass and glassceramic substrates were situ ated above the magnetron, and the stage was rotated during the sputterdeposition process to ensure trans verse homogeneity of the films. Prior to the deposition process, the vacuum chamber was pumped down to a residual pressure of 5×10^{-3} Pa. An appropriate mixture of argon and nitrogen gases was prepared directly during the deposition process using two independent gas sources. Unintentional

impurities (organic contamination and native oxide) on the target and substrate surfaces were removed by shortterm ion etching (bombard ment with argon ions). During the deposition process, the argon partial pressure in the vacuum chamber was 0.35 Pa and the nitrogen partial pressure was 0.7 Pa. The magnetron power was determined to be ~120 W. The deposition process was run for 15 min at a substrate temperature of ~570 K. The substrate temperature was monitored with a system of thermocouples situated in the vacuum chamber and was set by a controller on a control board. After the deposition process, the presence of TiN films on the substrates was evidenced by a change in the color of the substrate surface.

Electrical contacts for temperaturedependent electrical resistance (R) measurements were made on the opposite sides of the films through indium deposi tion at a substrate temperature of 400 K. R was mea sured as a function of T in the temperature range T = 295–420 K. Since irreversible processes, for example, oxidation, during temperaturedependent resistance measurements may change parameters of the film, the measurements were performed during both heating and cooling. Samples for Hall effect and electrical conductivity measurements had four Hall contacts and two Ohmic current contacts, which were made by indium thermal deposition through a mask. Transport coefficients were measured at dc in a static magnetic field in the temperature range 77–340 K. The effect of galvano and thermomagnetic side (parasitic) effects on mea surement results was eliminated by averaging mea surement results obtained at different current and magnetic field directions. The current through the sample was 10 μA, and the magnetic field was H = 5 kOe.

The net uncertainty in electrical conductivity was 2% and that in the Hall coefficient was 6%. The uncertainty in thermoelectric power was within 6%.

Electrical properties. When TiN is formed, each nitrogen atom, whose outer shell contains five valence electrons, gives them away to form chemical bonds with its nearest neighbors. Each titanium atom, whose outer shell contains four valence electrons, gives away three electrons to form covalent bonds with nitrogen (Ti–N), and the fourth valence electron proves to be redundant; that is, it is not involved in covalent bond formation . Because of the high dielectric per mittivity of the medium, the Coulomb interaction between this excess electron and the nucleus is weak ened to a significant degree. Even small thermal tation is sufficient to detach the excess electron from the Ti atom. Accordingly, these electrons produce shallow donor levels in the band gap of TiN, and a low activation energy is needed to promote them to the conduction band. For this reason, TiN contains high concentration of conduction electrons, proportional to the concentration of Ti atoms. Since 1 cm3 of TiN contains 2.6×10^{22} Ti atoms, the electron concentra tion should also be $\sim 10^{22}$ cm^{-3}, which is confirmed by experimental Hall effect and conductivity data (Fig. 1.9, insets a and b), $n = 2.88 \times 10^{22}$ $см^{-3}$ at room tempera ture, in good agreement with previous results. Giv ing away an electron, a titanium atom converts into a positively charged particle (ion), which resides on a lattice site, and, together with the other titanium ions and electrons, creates metallic bonding in TiN . Since titanium nitride has both metallic and cova lent (Ti–N) bonds, it can exhibit both metallic and semiconductor conductivity, in good agreement with data in the literature . The temperature dependence of the Hall coeffi cient RH= 1/(en) for the TiN thin films (Fig. 2, inset b) demonstrates that the conductivity of the films exhib its semiconducting behavior (R_H decreases with increasing T). The roomtemperature Hall coeffi cient, $R_H = -2.1 \times 10^{-4}$ $см^3$ /C, agrees well with data in the literature . Hall coefficient and thermoelectric power mea surements for the TiN thin films suggest that the trans port process involves electrons; that is, the TiN films are ntype. Figure 2 shows the temperature

dependence of resistance for the TiN thin films. It follows from these data that the electrical conductivity of the thin films under investigation exhibits semiconducting behavior. The measurements were made during both heating and cooling. It can be seen that heating produces no changes in the films, which indicates that the TiN thin films have high thermal stability, in contrast to TiO_2 films . The activation energy evaluated from the slope of the linear portion of the experimental R(T) curves for the TiN films is 0.15 eV and possibly corre sponds to the depth of a working energy level produced by the titanium's electron that is not involved in cova lent chemical bonding.

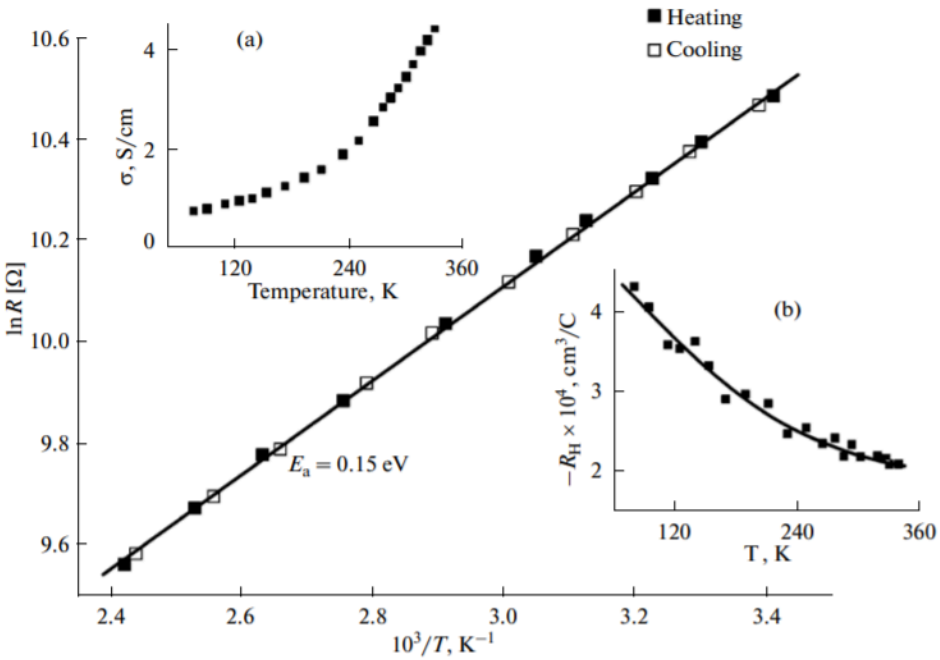

Fig. 1.9. Arrhenius plot of resistance for TiN films. Insets: temperaturedependent (a) electrical conductivity and (b) Hall coeffi cient of the films.

1.1.5. Electrical and photoelectrical properties of solar cells based on InP

Over the last two decades, organic thin-film devices, such as organic light-emitting diodes, organic thin-film transistors, photodetectors, and solar cells, have made steady progress in device performance with ever increasing range of applications . By many workers , it has been carried out their fabrications and electrical/optical characterizations of solar cells by using organic semiconductors. Organic semiconductors show many unusual electrical, optical, and magnetic properties, which could be used for the fabrication of molecular electronic devices . These materials also offer low cost and processing ease and can attain new roles not realized by conventional solar cells This has opened a new possibility of replacing conventional inorganic devices by the organic ones. Among those, methyl-red is considered a good candidate for organic semiconductor device fabrication such as photoelectric converters and solar cells. Methyl-red with molecular formula NC_6H_4COOH (dimethylamino)phenylazo] benzoic acid) used in this study is a typical aromatic azo compound. Its colour originates from absorbance in the visible region of the spectrum due to the delocalization of electrons in the benzene and azo groups forming a conjugated system. Due to its conjugated structure and richness in 16 π electrons, the methyl-red has been chosen to form an organic semiconductor layer between Al and p-InP inorganic semiconductor substrate. The molecular structure of the methyl-red is given in Figure 1.10 (a). The structure of azo dyes has attracted considerable attentions recently due to their wide applicability in the lightinduced photo isomerization process and their potential usage for the reversible optical data storage .Our aim is to investigate the electrical properties of Al/methyl-red/p-InP solar cell by the insertion of methylred organic layer between InP semiconductor and Al metal by using and current-voltage (I-V) and capacitance-voltagefrequency (C-V-f) measurements in dark and is to compare the electrical parameters of the

Al/methyl-red/p-InP solar cell with those of conventional Metal/Semiconductor diodes.

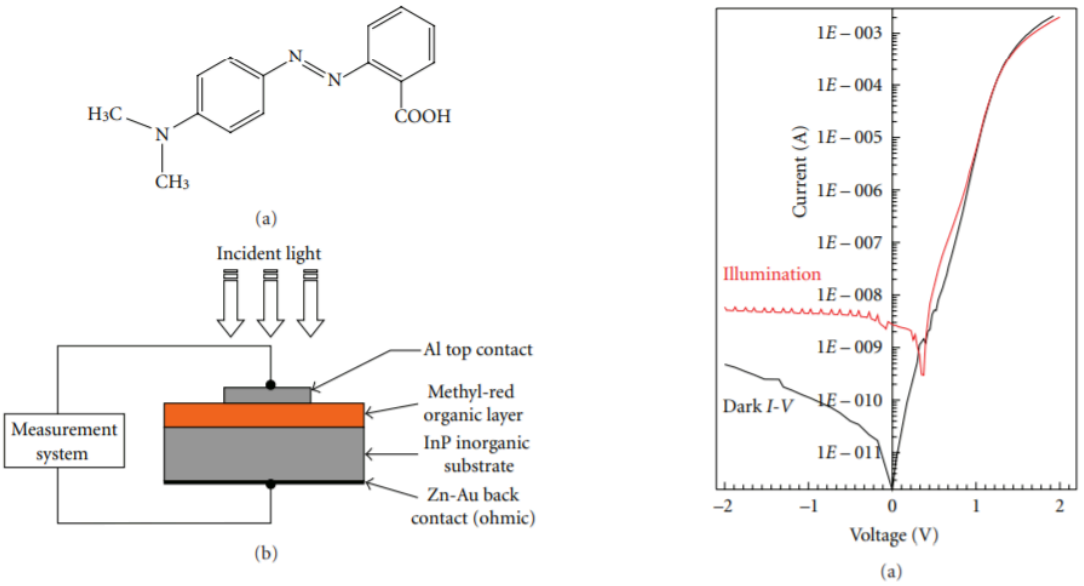

Figure 1.10: (a) Molecular structure of the methyl-red organic compound. (b) (Color online) The experimental setup of the Al/methyl-red/p-InP Schottky solar cell for the electrical and photovoltaic characterization.

1.1.6. Fabrication of solar cells based on heterojunctions

Heterojunction solar cells were formed with a position-controlled InP nanowire array sputtered with indium tin oxide (ITO). The ITO not only acted as a transparent electrode but also as forming a photovoltaic junction. The devices exhibited an open-circuit voltage of 0.436 V, short-circuit current of 24.8 mA/cm^2, and fill factor of 0.682, giving a power conversion efficiency of 7.37% under AM1.5 G illumination. The internal quantum efficiency of the device was higher than that of the world-record InP cell in the short wavelength range. According to the Shockley–Queisser limit, the maximum achievable efficiency for a single junction solar cell is ~33.2% which corresponds

to a bandgap (E_g) of 1.35 eV (InP). However, the maximum reported efficiency for InP solar cells remain at 24.2% ± 0.5%, that is >25% below the standard Shockley–Queisser limit. Through a wide range of simulations, we propose a new device structure, ITO/ ZnO/i-InP/p^+ InP (p-i-ZnO-ITO) which might be able to fill this efficiency gap. Our simulation shows that the use of a thin ZnO layer improves passivation of the underlying i-InP layer and provides electron selectivity leading to significantly higher efficiency when compared to their n^+/i/p^+ homojunction counterpart. As a proof-of-concept, we fabricated ITO/ZnO/i-InP solar cell on a p^+ InP substrate and achieved an open-circuit voltage (V_{oc}) and efficiency as high as 819 mV and 18.12%, respectively, along with ~90% internal quantum efficiency. The entire device fabrication process consists of four simple steps which are highly controllable and reproducible. This work lays the foundation for a new generation of thin film InP solar cells based solely on carrier selective heterojunctions without the requirement of extrinsic doping and can be particularly useful when p- and n-doping are challenging as in the case of III–V nanostructures
.

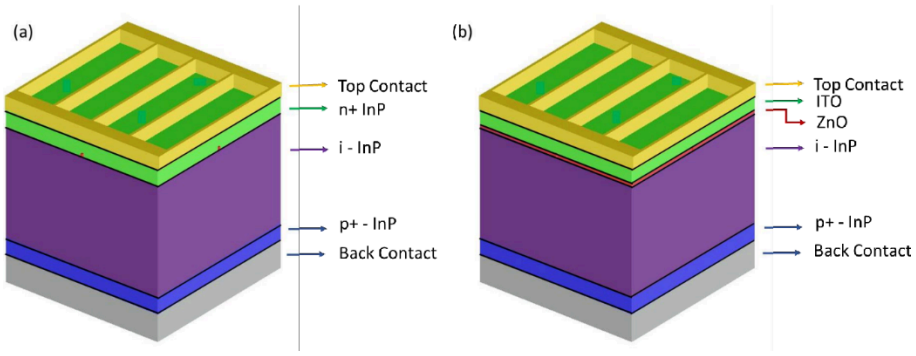

Figure 1.11. Schematic representation (not to scale) of the InP solar cell structures used for simulation (a) p-i-n and (b) p-i-ZnO-ITO. In both the figures, interface between two subsequent layers has been marked using a thin black line.

Graphene based van der Waals heterostructure has attracted wide attention recently, especially for graphene/semiconductor Schottky junction. Herein, through delicately designing and engineering the van der Waals heterostructure between graphene and indium phosphide (InP), which has a suitable bandgap of 1.34 eV for solar energy conversion, we have achieved graphene/p-InP solar cells with power conversion efficiency (PCE) of 3.3% under AM 1.5G illumination. The chemical doping or electrical field modulation has been used to tune the Fermi level of graphene, which leads to a PCE of 5.6% for the device under gating effect. Furthermore, the interface recombination rate could be reduced while graphene is doped or gated, as evidenced by transient photoluminescence measurements. Considering the stability of cell performance under illumination and the high resistance to space irradiation damage of InP, graphene/InP heterojunction may be promising for special applications such as space solar cells.

1.1.7. Methods of creating ohmic contacts to solar cells

An ohmic contact is a non-rectifying electrical junction: a junction between two conductors that has a linear current–voltage (I-V) curve as with Ohm's law. Low resistance ohmic contacts are used to allow charge to flow easily in both directions between the two conductors, without blocking due to rectification or excess power dissipation due to voltage thresholds.

By contrast, a junction or contact that does not demonstrate a linear I-V curve is called non-ohmic. Non-ohmic contacts come in a number of forms, such as p–n junction, Schottky barrier, rectifying heterojunction, or breakdown junction. Generally the term "ohmic contact" implicitly refers to an ohmic contact of a metal to a semiconductor, where achieving ohmic contact resistance is possible but requires careful technique. Metal–metal ohmic contacts are relatively simpler to make, by ensuring direct contact between the metals without intervening layers of

insulating contamination, excessive roughness or oxidation; various techniques are used to create ohmic metal-metal junctions (soldering, welding, crimping, deposition, electroplating.). This article focuses on metal–semiconductor ohmic contacts.

Stable contacts at semiconductor interfaces, with low contact resistance and linear I-V behavior, are critical for the performance and reliability of semiconductor devices, and their preparation and characterization are major efforts in circuit fabrication. Poorly prepared junctions to semiconductors can easily show rectifying behavior by causing depletion of the semiconductor near the junction, rendering the device useless by blocking the flow of charge between those devices and the external circuitry. Ohmic contacts to semiconductors are typically constructed by depositing thin metal films of a carefully chosen composition, possibly followed by annealing to alter the semiconductor–metal bond.

selective contact of a solar cell with metal leads connecting to external load. This chapter is devoted to the concept of ideal ohmic contacts and to realization principles of ohmic contacts at metal–semiconductor and semiconductor–semiconductor interfaces. Barriers are formed at metal–semiconductor interfaces depending on the metal work function, the electron affinity, doping of the semiconductor and interfacial defects. High densities of interface defects cause Fermi-level pinning. Tunneling of free charge carriers through very thin barrier layers at highly doped semiconductors is decisive for ohmic contacts in solar cells with very high solar energy conversion efficiencies. The transmission probability is derived for a triangular barrier the width and height of which are given by the extension of the space charge region and by the barrier at the contact, respectively. The tunneling or contact resistance is obtained as a function of the barrier height and of the density of dopants in a highly doped semiconductor. Consequences for the tolerable series

resistance and design of solar cells are discussed. Furthermore, tunneling contacts are considered between a highly doped n-type and a highly doped p-type semiconductor for integrated series connection in multi-junction solar cells. Ohmic contacts may be realized as well by defect-assisted tunneling through barrier layers.

SECTION 2. Results and discussion

2.1. Solar cell configuration development

Currently different prospective semiconductor materials and structures based on them are under intensive research for their application in electronics and photovoltaics. The application of heterojunctions for the fabrication of photoelectrical converters enhances their operational characteristics comparing with that of photoelectrical devices based on homojunctions

Titanium nitride thin films find their wide application in different semiconductor devices due to the optimal combination of physical and chemical parameters: low specific resistance, high transparency within the visible range, high reflectance in the infrared part of spectrum, high hardness, high wear resistance, good chemical inertness and resistance to corrosion.

The use of an InP thin film solar cell is proposed; its qualities of high efficiency and high radiation resistance are important in minimizing cost and weight. The advantages of InP over GaAs and Si as a thin film solar cell material are discussed. The photovoltaic properties of the InP thin film solar cell are calculated by considering the dislocation effect upon the minority-carrier diffusion length in the thin film. It is estimated that one can fabricate InP thin film solar cells on Si substrates, with an efficiency of 18% or more, if the dislocation density in the InP film is less than 10^6 cm^{-2}.

Due to their properties TiN and InP are prospective materials for the application in different photoelectrical devices. Therefore, the fabrication and characterization of heterojunctions TiN/InP/Graphite are of great interest. The large

value of the band gap of titanium nitride provides the efficient absorption of sun light in InP and, thus, high photosensitivity of the semiconductor heterostructure TiN/InP/Graphite within the wide spectral range. Also due to the radiation and chemical resistance of the components of the heterojunction such devices can be used as detectors of different types of radiation for a continuous operation in aggressive environment and under elevated level of radiation.

Fig.2.1. Block diagram of the investigated solar cell TiN / InP / graphite

Before experimental techniques will be coupled with advanced numerical simulation methods to comprehensively understand the photoelectric processes in the studied novel solar cell based TiN/InP/Graphite heterojunction (Fig. 2.1). In particular, we are planning to employ well-established transfer matrix and drift-diffusion models for optical and electrical simulations, respectively. These complementary numerical simulation techniques will provide detailed information on the space- and wavelength-dependent photogeneration rate of free charge carriers and their transport within the active layer.

2.2. Optical Properties all Layer for Simulation of the Generation Rate in the Active Layer

Thickness measurements are not independent of the optical constants. The film thickness affects the path length of light traveling through the film, but the index determines the light waves' velocity and refracted angle. Thus, both contribute to the delay between surface reflection and light traveling through the film. Both n and k must be known or determined along with the thickness to get the correct results from an optical measurement.

The optical constants for a material will vary for different wavelengths and must be described at all wavelengths probed with the ellipsometer. A table of optical constants can be used to predict the material's response at each wavelength. However, it is not very convenient to adjust unknown optical constants on a wavelength-by-wavelength basis. It is more advantageous to use all wavelengths simultaneously. A dispersion relationship often solves this problem, by describing the optical constant shape versus wavelength. The adjustable parameters of the dispersion relationship allow the overall optical constant shape to match the experimental results. Compared to fitting individual n, k values at every wavelength, this greatly reduces the number of unknown "free" parameters.

For transparent materials, the index is often described using the Cauchy or Sellmeier relationship. The Cauchy relationship is typically given as:

$$n(\lambda) = A + \frac{B}{\lambda^2} + \frac{C}{\lambda^4} \tag{2.1}$$

where the three terms are adjusted to match the refractive index for the material. The Cauchy is not constrained by KK consistency and can produce unphysical dispersion. The Sellmeier relationship enforces Kramers-Kronig (KK) consistency, which ensures that the optical dispersion retains a realistic shape. The Sellmeier relationship can be written as:

$$\varepsilon_1 = + \frac{A\lambda^2\lambda_0^2}{\left(\lambda^2 - \lambda_0^2\right)} \tag{2.2}$$

Absorbing materials will often have a transparent wavelength region that can be modeled with the Cauchy or Sellmeier. However, the absorbing region must account for both real and imaginary optical constants. Many dispersion relationships use oscillator theory to describe absorption for various materials. These include the Lorentz, Harmonic, and Gaussian oscillators. They all share similar attributes, where the absorption features are described with an Amplitude, Broadening, and Center Energy (related to frequency of light). Kramers-Kronig consistency is used to calculate the shape of the real component after the imaginary behavior is described by the oscillator. An offset to the real component is added to account for extra absorption outside the measured spectral region. The Lorentz oscillator can be written as:

$$\varepsilon = \varepsilon_{1\,offset} = + \frac{AE_c}{E_c^2 - E^2 - iBE} \tag{2.3}$$

where the parameters for Amplitude (A), Broadening (B), Center Energy (Ec), and offset (e1, offset). The energy, E, is related to the frequency of a wave, n:

$$E = h\nu \cong \frac{1240}{\lambda_{nm}} \tag{2.4}$$

where h is Planck's constant and the wavelength, l, is given in nanometers. More advanced dispersion models, like the Tauc-Lorentz and Cody-Lorentz, will include terms to describe the bandgap energy.

Initially, the optical constants of all layers of the solar cell were found in the literature.

Figure 2 shows the spectral dependences n and k of of titanium nitride thin films. The refractive index *n* (λ) for the TiN films increases with increasing wavelength in the range λ > 500 nm, which is caused by the increase in reflectance in the infrared spectral region. The sharp rise in refractive index at wavelengths λ <

500 nm is due to the increase in reflectance near the fundamental absorption edge of the thin titanium nitride films.

The extinction coefficient can readily be found using the relation $k(\lambda) = \lambda\alpha(\lambda)/4\pi$. The extinction coefficient also rises sharply near the fundamental absorption edge of the films under investigation (Fig. 2.2, inset). At the same time, in the transmission window of the films ($\lambda > 500$ nm), we observe a slight increase in extinction coefficient, which is caused by the increase in absorption coefficient.

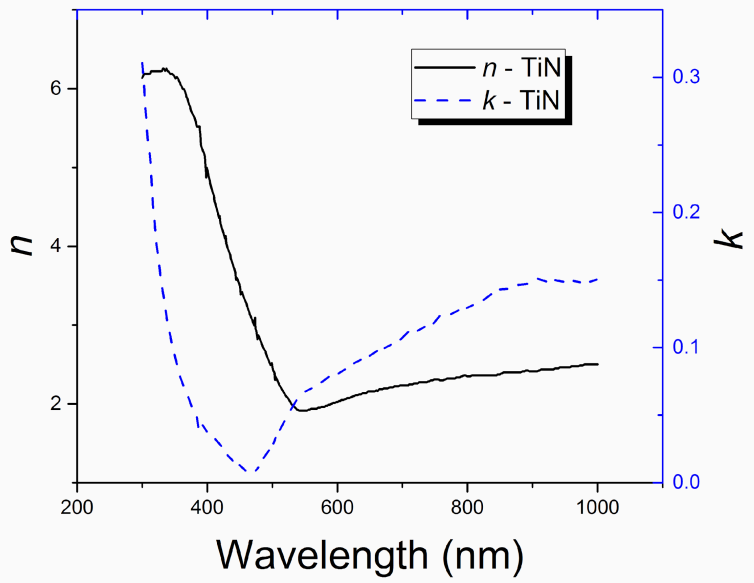

Fig. 2.2. Reflection and Extinction Coefficient spectra of TiN thin films

Figure 2.3 shows the spectral dependences n and k of of InP thin films.

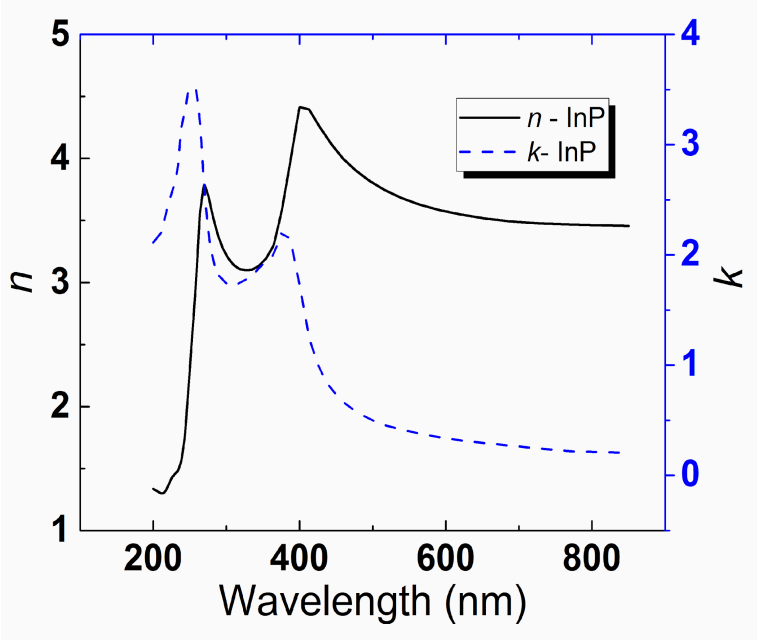

Fig. 2.3. Reflection and Extinction Coefficient spectra of InP thin films

As can be seen from Fig. 2.3, the refractive index first increases with increase in photon energy in the photon energy range 1.45 – 6.2 eV with a maximum value of 4.42 at 2.7eV. The extinction coefficient obtained for InP in the photon energy range 1.45 – 6.2 is shown in Fig. 2.3. As can be seen from Fig. 2.3, the extinction coefficient first increases with increase in photon energy in the photon energy range 1.45 – 3.2eV. It then drops and rises to a maximum value of 3.5 at 4.8eV and afterwards decreases with increase in photon energy. The increase in extinction coefficient with increase in photon energy in the photon energy range 1.45 – 3.2eV shows that the fraction of light lost due to scattering and absorbance increases in this energy range and the decrease in the extinction coefficient in the photon energy range 4.8 – 6.0eV shows that the fraction of light lost due to scattering and absorbance decreases in this energy region.

Figure 2.4 shows the spectral dependences n and k of of graphite thin films.

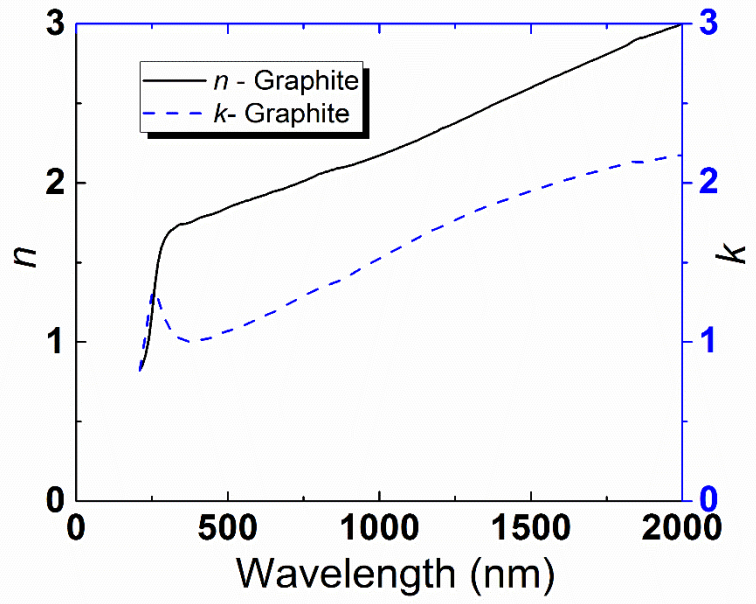

Fig. 2.4. Reflection and Extinction Coefficient spectra of graphite thin films

The dependence shows that the refractive index and extinction coefficient increase smoothly, due to the nature of the films.

2.3. Simulation of short-circuit current density depending on the thickness of the active layer.

For the operation of solar cells, it is important to generate electron-hole pairs when absorbing the energy of the Sun's radiation. The more electrons and holes will be generated, the greater the current of the solar cell can be. Electron-hole pairs are able to form light quanta with an energy hν that is proportional to or greater than the band gap Eg.

Figure 2.5 shows the dependence of the spectral intensity of solar radiation, which is measured in units of $W/m^2/nm$, on the wavelength of radiation λ (μm). Additionally, Figure 2.5 shows the axis with energy values according to the wavelength. The energy is calculated according to the given expression $h\nu = hc / \lambda$

to the dimensions hν (eV) and λ (μm), ie hν (eV) = 1.24 / λ (μm). To analyze the efficiency of the use of solar radiation in the generation of electron-hole pairs by vertical lines, the location of the band gap of InP (Eg = 1.45 eV) semiconductors, which are used as photoactive layers in photoconverters, and TiN (Eg = 3.4 eV), which is often used to make the front part of solar cells based on heterojunctions.

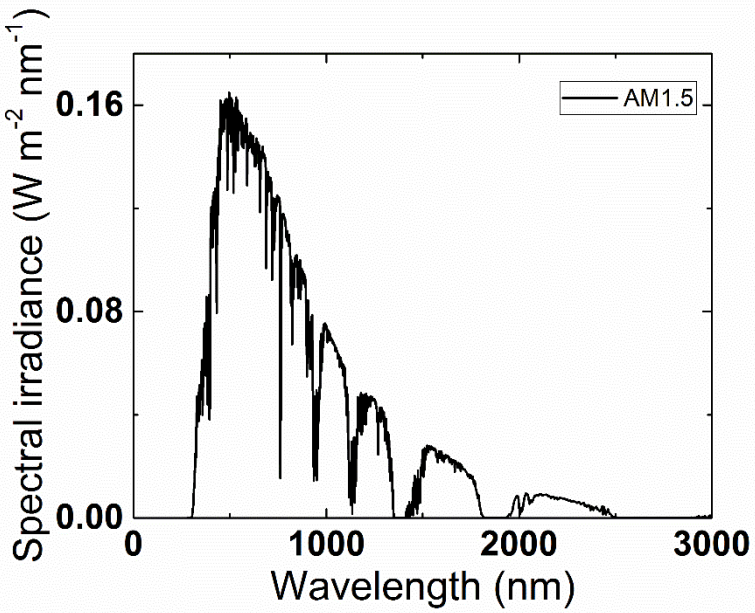

Fig.2.5. Spectral intensity of solar radiation.

Figure 2.6 shows short-circuit current density depending on the thickness of the active layer. Which was simulated based on the optical properties of all layers of the solar cell and the spectral dependence of solar radiation.

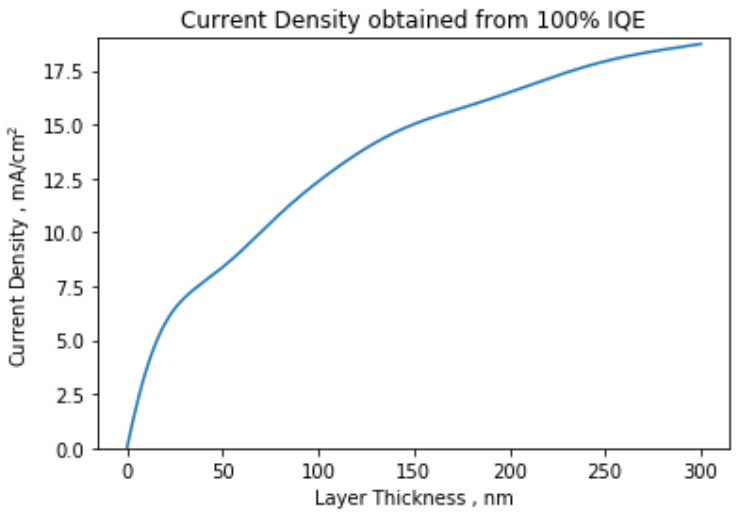

Fig. 2.6. Calculation of the short-circuit current density from the thickness of the absorber (InP)

The figure 2.6 shows that at a thickness of 300 nm, the current density reaches maximum values. Therefore, we will longer use the thickness of the active layer equal to 300 nm for calculations.

2.4. Simulation of the Generation Rate in the Active Layer

Based on the optical properties of all layers, the spectral dependences of absorption, transmission and reflection on the solar cell are calculated (Fig 2.7).

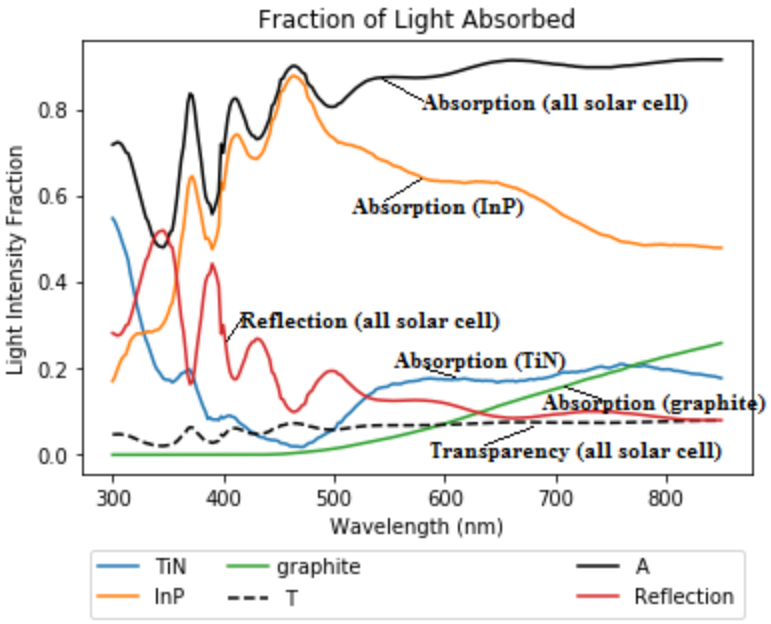

Fig. 2.7. Calculated optical properties of the solar cell TiN/InP/Graphite

The reduced absorption of photons in the more transparent devices directly results in reduced generation rates and hence reduced charge generation rates. The charge generation rates $G(x, \lambda)$, in dependence on the position x in the active layer (illumination from $x = 0$ side at normal incidence) and the wavelength λ, are simulated with the optical transfer matrix method and are shown in Figure 8, based on the device architectures and the optical constants of each layer. The resulting 3D-generation rate profiles visualize the effect of an increased AVT on the charge carrier generation under 1 sun AM1.5 illumination. First, the expected reduction of the generation rate in the visible range with increased transparency is apparent. Second, the effects of the reflective Graphite back electrode can be seen.

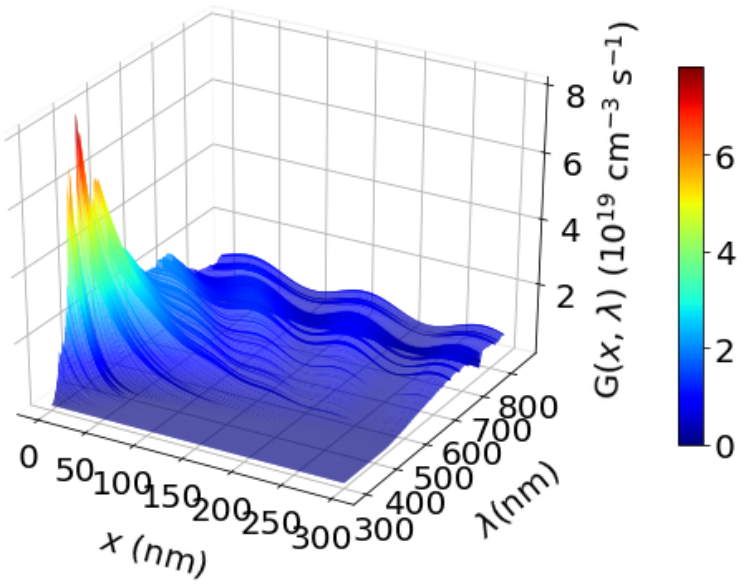

Fig. 2.6. The rate of generation of charge carriers depending on the wavelength of the incident light on the thickness of the absorber

To be able to compare the resulting generation rates, we show the spatially dependent charge generation rate $G(x)$, that is calculated as $\int_{\lambda}^{\lambda`} G(x, \lambda)d\lambda = G(x)$, in Figure 9. This plot demonstrates that the strongly reduced backside reflection, caused by the close match of the refractive indices of the active layer and TiN, leads to a reduction of $G(x)$ (maximum 1.4×10^{22} cm^{-3} s^{-1}). The reduction of the absorption in the active layer reduces $G(x)$ further by approximately one order of magnitude (maximum at 0.2×10^{22} cm^{-3} s^{-1} for the *k* 0 device).

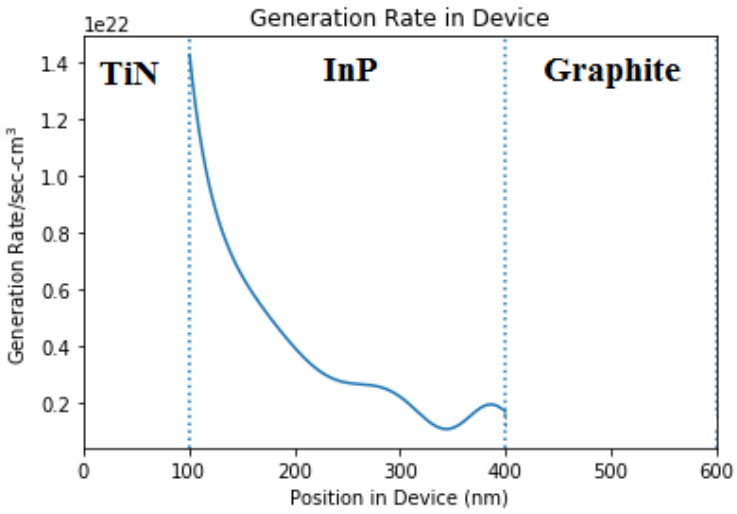

Fig.2.9. Simulated spatially dependent generation rate G(x) for AM1.5 illumination reveal changes in the spatial distribution

2.5. Quantum efficiency and sensitivity of solar cells

The spectral distribution of the apparent quantum efficiency $\eta(\lambda)$ was calculated as the ratio of the number of charge carriers that form the short-circuit current to the number of photons of a fixed energy impinging on the TiN/InP/Graphite heterojunction from the side of the TiN thin film per unit time. It is characterized by the band's width $\delta_{1/2}$ = 0.5 μm at its half-height (figure 2.10).

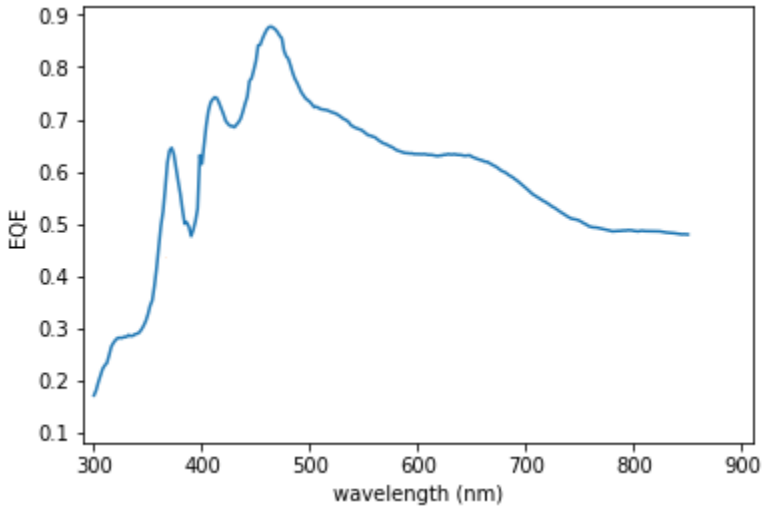

Fig. 2.10 The total quantum efficiency of the solar cell is calculated

The spectral distribution of the quantum efficiency of the TiN/InP/Graphite heterojunction is well correlated with the transmittance of the TiN thin film within the short wavelength region (figure 10). The absence of the sharp short wavelength edge in the mentioned spectra is due to the small thickness of the TiN thin film and its polycrystalline structure.

The figure shows the calculations of the sensitivity of the solar cell to incident radiation. It is possible to estimate productivity of a solar element more quantitatively by means of definition of sensitivity (R) which reflect sensitivity of a photodetector to incident radiation:

$$R = \left(I_{light} - I_{dark}\right) / P_{opt}\,, \tag{2.12}$$

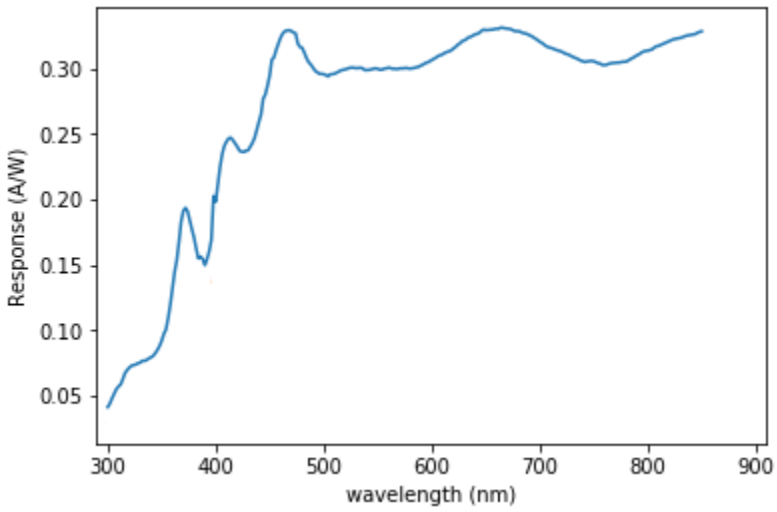

Fig. 2.11. Sensitivity of the solar cell to incident radiation

In fig. 2.11 shows R = f (λ) from which it can be seen that the sensitivity (R) increases sharply with increasing wavelength from 300 nm to 450 nm, and the maximum sensitivity values reach 0.3 A/W.

Conclusion

1. Solar elements based on TiN/InP/graphite structures are proposed.

2. The rate of photogeneration of free charge carriers depending on the absorber thickness and wavelength in solar cells TiN/InP/graphite is determined

3. It is established that in solar cells based on TiN/InP/graphite the optimal thickness of the absorber (InP) is 300 nm.

3. Solar cells demonstrates that the strongly reduced backside reflection, caused by the close match of the refractive indices of the active layer and TiN, leads to a reduction of $G(x)$ (maximum 1.4×10^{22} cm^{-3} s^{-1}). The reduction of the absorption in the active layer reduces $G(x)$ further by approximately one order of magnitude (maximum at 0.2×10^{22} cm^{-3} s^{-1} for the k 0 device).

4. It is shown that the solar cells TiN/InP/graphite will have a wide range of spectral sensitivity (from 300 to 850 nm).

References

[1] K.T. Chaudhary, R. Qindeel, Saktioto , M.S. Hussain, J. Ali and P.P. Yupapinf Graphite Thin Film Deposition using Laser Induced Plasma Procedia Engineering 8 (2011) 423–427

[2] M.M. El-Nahass, S.B. Youssef, H.A.M. Ali Optical properties of Sulfur doped InP single crystals Physica A 402 (2014) 216–223

[3] Würfel, P. Physics of Solar Cells: From Principles to New Concepts; Wiley: Weinheim, Germany, 2005.

[4]Shrotriya, V.; Li, G.; Yao, Y.; Chu, C.-W.; Yang, Y. Transition metal oxides as the buffer layer for polymer photovoltaic cells. Appl. Phys. Lett. 2006, 88, 073508.

[5]Xie, F.; Choy, W. C. H.; Wang, C.; Li, X.; Zhang, S.; Hou, J. Lowtemperature solution-processed hydrogen molybdenum and vanadium bronzes for an efficient hole-transport layer in organic electronics. Adv. Mater. 2013, 25, 2051−2055.

[6]Sun, Y.; Takacs, C. J.; Cowan, S. R.; Seo, J. H.; Gong, X.; Roy, A.; Heeger, A. J. Efficient, air-stable bulk heterojunction polymer solar cells using MoOx as the anode interfacial layer. Adv. Mater. 2011, 23, 2226−2230.

[7] Irwin, M. D.; Buchholz, D. B.; Hains, A. W.; Chang, R. P. H.; Marks, T. J. p-Type semiconducting nickel oxide as an efficiencyenhancing anode interfacial layer in polymer bulk-heterojunction solar cells. Proc. Natl. Acad. Sci. U.S.A. 2008, 105, 2783−2787.

[8]Chen, C.-P.; Chen, Y.-D.; Chuang, S.-C. High-performance and highly durable inverted organic photovoltaics embedding solutionprocessable vanadium oxides as an interfacial hole-transporting layer. Adv. Mater. 2011, 23, 3859−3863.

[9]Tao, C.; Ruan, S.; Xie, G.; Kong, X.; Shen, L.; Meng, F.; Liu, C.; Zhang, X.; Dong, W.; Chen, W. Role of tungsten oxide in inverted polymer solar cells. Appl. Phys. Lett. 2009, 94, 043311.

APPENDIX A. Safety and labor protection

1.1. Work with electrical meters and high voltage

1.1.1. Safety precautions when working with electrical measuring instruments

Before starting to work it is necessary:

- To study the basic and assembly schemes of the equipment which is subject to regulation;
- Get the necessary measuring equipment, make sure it is working;
- Check the condition of the workplace;
- Remove from the workplace unnecessary items that interfere with work;
- Position the lamp so that the work area is well lit and the light does not blind the eyes;
- Make sure the availability and serviceability of protective equipment;
- To be convinced of serviceability of isolation of wires, connecting blocks, plug sockets and plugs;
- To check up serviceability of protective grounding of the repaired and measuring devices;
- To be convinced of serviceability of starting, blocking and signaling devices;
- Make sure that all toggle switches, switches and circuit breakers are in the "off" position.

Work safety requirements:

- Maintain cleanliness and order in the workplace;
- Perform only the work assigned by the teacher;

- When working without de-energizing it is necessary to use a tool with insulated handles;

- When working with the voltage on, work on the equipment is allowed only with one hand, avoiding contact with the other hand (and exposed body parts) of equipment, chassis, metal housings, as well as measuring instruments in metal housings;

- Connection of the measuring equipment is necessary for carrying out at the de-energized block;

- It is allowed to measure voltage up to 1000 V on the switched on equipment by touching the high-voltage probe or voltage divider included in the measuring instrument, the point, the potential of which must be set. During such measurements, the safety measures provided for in the operating instructions of the measuring instrument must be taken;

- When replacing parts, the equipment should be disconnected from the mains;

- At short breaks in work the soldering irons which are in a working condition, it is necessary to place on a special support. During long breaks, the soldering iron must be disconnected from the mains;

- When leaving the workplace, repaired equipment and measuring instruments should be turned off.

Safety requirements after work:

- Put switches, toggle switches, switches in the "off" position;

- Disconnect the testing equipment and measuring instruments from the network;

- Clean the workplace, tools, devices and protective equipment;

- Present the work done to the teacher.

1.1.2. Safety precautions when working with high voltage

- It is necessary to carry out various electrical work only when the entire network is de-energized. This axiom must be followed, even when performing the simplest procedure to replace a blown light bulb at home.

- When servicing or repairing high voltage equipment, it is necessary to use tools covered with insulating material. An experienced specialist should pay attention to the calculation of cable power and network differences.

- Work should be done only with dry hands. It is necessary to exclude water getting into the installation area.

- When replacing fuses, never insert metal objects into the socket to avoid electric shock or severe burns.

- In the event of an emergency, the fire must not be extinguished with water. First of all the device should be disconnected from current, and then already to liquidate.

1.2. Fire Security

General fire safety requirements:

- Everyone should know the rules of conduct in case of fire, evacuation routes, be able to use primary means of firefighting, know their location;

- Flammable and combustible liquids must be stored in specially designated areas separately from other materials.

Rules of conduct for people in case of fire:

- In case of fire, it is necessary to call a specialized fire department by phone 101 and notify neighbors, company management, colleagues and immediately begin to eliminate the fire by all available means;

- Take the necessary measures to extinguish the fire on their own;

- Evacuate people and property. First of all, the most valuable and flammable materials are evacuated;

- If it is impossible to extinguish the fire on their own, you need to leave the room as soon as possible through the main and emergency exits;

- Leaving the room where the fire broke out, close the door tightly to reduce the flow of oxygen to the room.

Evacuation of people in case of fire

An indicator of the effectiveness of the evacuation process is the period of time during which people can, if necessary, leave individual rooms and the house in general.

Evacuation safety is achieved when the duration of evacuation of people from individual rooms and the house as a whole is less than the critical duration of a fire that poses a danger to humans.

The critical duration of a fire is the time to reach dangerous human temperatures and reduce the oxygen content in the air.

The main danger from which people die in fires is smoke and hot air, so in a smoky room you need to breathe only through a wet dense cloth, remembering that the concentration of smoke is lowest near the floor.

Primary fire extinguishers are placed on special boards. Shields are installed so that the farthest building is not more than 100 m, and from storage facilities with flammable materials - not more than 50 m, or at the rate of - one shield per 5000 m2.

Fire extinguishers are painted in signal red, and the inscriptions on them and on the shields are made in contrasting white.

1.3. Basic measures when working with chemicals

Working with chemical reagents is a dangerous type of work, as chemicals can actively affect people and technology. Therefore, compliance with safety rules is the most important condition for the work.

When dealing with chemicals, keep in mind the following:

- Service personnel who have contact with chemical reagents must undergo preliminary (at the time of entry into employment) and periodic medical examinations (once a year);

- Admission to work with chemicals of pregnant women, adolescents under 18 years, patients with organic skin lesions, chronic diseases of internal organs, central nervous system, upper respiratory tract, visual organs is prohibited;

- Persons who have been specially instructed on safety measures when working with flammable and toxic substances are allowed to work with reagents;

- The room in which the work with the chemical reagent is carried out, must be equipped with general exchange supply and exhaust ventilation, local exhausts in places of possible accumulation of vapors;

- It is forbidden to pour the product near heat sources, sparks, open flames;

- Wet cleaning of working premises should be carried out regularly.

- Chemicals must be stored in closed containers in warehouses, semi-closed type;

- In rooms for storage and use of chemical reagents it is forbidden to use open fire, and also to use the tools giving at blow by a spark;

- When working with the product, observe fire safety measures, safety measures, use personal protective equipment. Overalls must withstand the effects of chemical reagents;

- Use safety goggles such as GR, rubber gloves, waterproof gloves, special shoes, use a BKF filter gas mask;

- The workplace should be equipped with a first aid kit containing neutralizers for the solution with which you have to work, and a supply of fresh water;

- When using methyl alcohol and products that contain methyl alcohol, take special precautions;

- When dosing or draining chemical solutions, staff must be on the windward side;

- Symptoms of poisoning: headache, dizziness, vomiting, abdominal pain, general weakness, irritation of the mucous membranes, flickering in the eyes;
- Acids are the most dangerous substances: they destroy the surface layer of tissue, cause burns to the point of charring the skin, affect the eyes, affect the respiratory system;
- Alkalis cause saponification of the fatty layer of the skin, dehydration of tissues, dissolution of proteins.